Ban. J. Med. Phys., Vol -16, Issue -1, 2025 : 24-29

ORIGINAL ARTICLE

BANGLADESH JOURNAL OF MEDICAL PHYSICS

Journal Homepage: www.banglajolinfo/index.php/bjmp

Production of the ^{169}Er Radionuclide Via Deuteron-Induced Reaction on ^{168}Er: A Theoretical Study

Sukarna Banik[1], Md. Kawchar Ahmed Patwary*[1], Quazi Muhammad Rashed Nizam[2], Jannatul Fardous[3], Maria Sultana[1], Hasan Murad[4]

[1]*Department of Physics, Comilla University, Cumilla 3506, Bangladesh*

[2]*Department of Physics, University of Chittagong, Chattogram 4331, Bangladesh*

[3]*Department of Pharmacy, Comilla University, Cumilla 3506, Bangladesh*

[4]*Department of Physics, Cumilla Victoria Govt. College, Cumilla 3500, Bangladesh*

ARTICLE INFO

Article history:
Received :
Received in revised form :
Accepted :
Available online :

Key words: Radiosynovectomy, ^{169}Er radionuclide, ^{168}Er(d,p)^{169}Er reaction, TALYS-2.0, accelerator-based production, nuclear model.

doi: https://doi.org/10.3329/bjmp.v16i1.84800

Article Category: Isotop Production

***Corresponding author:**

Md. Kawchar Ahmed Patwary
e-mail: kapphysics@cou.ac.bd

ABSTRACT

This study evaluates the ^{168}Er(d,p)^{169}Er reaction for accelerator-based production of ^{169}Er($t_{1/2}$ 9.39d), a radionuclide widely applied in radiosynovectomy (RSV). Excitation functions were calculated up to 200 MeV using TALYS-2.0, considering six level density models, optical model, and mass model. A constant deuteron beam with the current of 5 mA irradiated a 0.025 mm thick ^{168}Er target foil having area of 25 mm × 25 mm for 24 hours. Results showed consistent cross-section predictions across models, with an optimal excitation function between 5–20 MeV. The maximum cross-section was 128 mb at ~9 MeV, yielding a peak activity of ~540 GBq at end of bombardment (EOB), corresponding to ~4.6 GBq/mA-h. Production amounts reached 6.32 × 10^{17} atoms, with post-irradiation decay following expected exponential trends. These findings confirm that the ^{168}Er(d,p)^{169}Er route offers a reliable, high-yield, and reactor-independent pathway for localized ^{169}Er production, enabling broader clinical access for RSV and potential therapeutic and post-RSV imaging applications.

1. Introduction

Erbium-169 (^{169}Er), a pure β^-emitter, is a clinically relevant radionuclide with promising applications in radionuclide therapy, particularly radiosynovectomy (RSV) for the treatment of rheumatoid arthritis and related disorders in small joints.[1-2] Administered in the form of ^{169}Er citrate, it delivers localized β^-radiation with minimal damage to surrounding tissues. With a half-life $t_{1/2}$=9.39 d, ^{169}Er emits two low-energy β^-particles E_{β^-max} = 343 keV, I_{β^-} = 45% and E_{β^-max} = 351 keV, I_{β^-} = 55%) along with a weak 109.8 keV γ-ray (as shown in **Fig. 1**), making it suitable for both therapy and post-RSV imaging.[3]

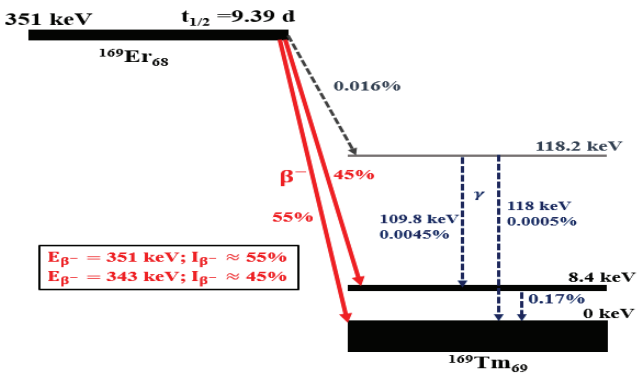

Fig. 1. Decay scheme of ^{169}Er.[4]

Traditionally, ^{169}Er is produced via the (n,γ) reaction, which requires high-flux neutron sources from nuclear reactors.[5,6] This route typically involves irradiation of highly enriched $^{168}Er_2O_3$ targets; however, the relatively low neutron capture cross section of ^{168}Er (σ_{cap}= 2.3 barn[7]) limits the specific activity of ^{169}Er in carrier-added form. Reported specific activity include ~240 GBq/mg from mass-separated ^{169}Er and approximately 370 MBq/mg (or, 10 mCi/mg) in other studies.[5,6] In addition, reactor-based production introduces radionuclide impurities such as 1% ^{169}Yb, with further complications arising from the co-production of long-lived ^{169}Yb ($t_{1/2}$= 32 d) due to trace ^{168}Yb in enriched targets.[5,8] These challenges underscore the need for alternative production routes to ensure cost-effective availability of ^{169}Er with high specific activity and adequate production yield for clinical applications in RSV.

Accelerator-based production of medical radionuclide has recently gained attention due to its feasibility for on-site production and compatibility with modern radiopharmaceutical development facilities. Despite these advantages, comprehensive accelerator-based studies on ^{169}Er production remain scarce, and no measurements are currently available in the IAEA databases, EXFOR.[9] This lack of data limits the optimization and standardization of accelerator-based ^{169}Er production.

Therefore, the present study investigates an accelerator-based production route for ^{169}Er via the ^{168}Er(*d,p*)^{169}Er reaction. Using TALYS-2.0, a nuclear reaction modeling code[10], theoretical simulations were carried out to evaluate the excitation function of the ^{168}Er(*d,p*)^{169}Er reaction at deuteron energies up to 200 MeV. Furthermore, the cross-section profile, activity, production amount, and yield of ^{169}Er were assessed to provide a comprehensive understanding of its accelerator-based production potential.

2. Analytical Approach to Nuclear Data Evaluation

2.1 TALYS-2.0

TALYS-2.0, a nuclear reaction calculation code that incorporates an optimized combination of reliable nuclear models was utilized for investigating the production of ^{169}Er via the ^{168}Er(*d,p*)^{169}Er reaction to simulate interactions up to 200 MeV incident deuteron energies.[10] A comprehensive evaluation of the excitation function, production amount, yield, and activity of ^{169}Er is essential for understanding reaction mechanisms and their practical applications. For these calculations, we have set the interaction modes, level density models, optical model parameters, and mass model parameters in TALYS-2.0. The following sub-sections outlines the rationale behind the choice of these parameters and their role in determining optimal values within TALYS-2.0.

2.2 Nuclear Level Density Models and Parameter Adjustment

Nuclear level density models play a key role in statistical reaction calculations, as they strongly influence the optimized production of radionuclides.[11] To achieve accurate predictions, several parameters in TALYS-2.0 must be carefully adjusted, including *rvadjust*, *avadjust*, *v1adjust*, *v2adjust*, *v3adjust*, *v4adjust*, *rwadjust*, and *awadjust*. The *rvadjust* parameter modifies the nuclear radius in the optical potential, affecting the spatial extent of nuclear interactions and the overall cross-section magnitude. *avadjust* changes the level density parameter, which governs the number of available nuclear states at higher excitation energies and directly impacts compound nucleus formation and decay probabilities. *v1adjust* and *v2adjust* control the depth of the optical potential volume terms, determining how strongly a projectile interacts with the target nucleus and how deeply it penetrates before reacting. Similarly, *v3adjust* and *v4adjust* fine-tune the surface terms of the optical model, which are particularly important for reactions occurring at the nuclear boundary, such as scattering. *rwadjust* alters the radius of the spin–orbit potential, refining how spin–orbit interactions are spatially distributed, while *awadjust* modifies its depth, adjusting the strength of spin–orbit coupling that governs angular distributions. Together, these parameters allow the theoretical models to be matched more closely with experimental data, improving the reliability of predicted cross-sections, yields, and reaction mechanisms.

Standard TALYS-2.0 offers six level density models for nuclear reaction analysis. The phenomenological models include the Constant Temperature Model (CTM), Back-Shifted Fermi Gas Model (BFM), and Generalized Superfluid Model (GSM), all derived from the Fermi Gas Model (FGM), which assumes uniformly spaced single-particle states without collective excitations.[10] The microscopic approaches consist of the Skyrme-Hartree-Fock-Bogolyubov (SHFB), the Combinatorial SHFB (a deformed SHFB with collective enhancement), and the Gogny-Hartree-Fock-Bogolyubov (GHFB). Arguably, the best-known analytical level density expression is FGM. Fermi gas level density can be expressed as Eq. (1).

$$\rho_F(E_x, J, \Pi) = \frac{1}{2}\frac{(2J+1)}{2\sqrt{2\pi}\sigma^3}\exp\left[-\frac{(J+\frac{1}{2})^2}{2\sigma^2}\right] \times \frac{\sqrt{\pi}}{12}\frac{\exp[2\sqrt{aU}]}{a^{\frac{1}{4}}U^{\frac{5}{4}}} \quad (1)$$

Here, the level density $\rho_F(E_x, J, \Pi)$ corresponds to the number of nuclear energy levels per incident particle energy in MeV near a given excitation energy E_x, for a particular spin J, and parity Π, and cross-section, σ, $a = \frac{\pi^2}{6}(g_\pi + g_\nu)$, with g_π and g_ν denoting the spacing of the proton and neutron single particle states near the Fermi energy, U is effective excitation energy $U=E_x-\Delta$. The energy shift, Δ is an empirical parameter that is either equal to or closely associated with the pairing energy in certain models. It is introduced to replicate the well-known odd-even effects observed in nuclei. The first factor $\frac{1}{2}$ represents the equipartition distribution and σ^2 is the spin cut-off parameter, which represents the width of the angular momentum distribution and depends on E_x.

2.3 Optical Model Parameters

An effective optical model can accurately predict key nuclear reaction quantities, including cross sections (elastic, inelastic, and total), angular distributions, and transmission coefficients for compound nucleus decay and pre-equilibrium emission, using either deformed nuclei or DWBA approaches.[12] In TALYS-2.0, optical model calculations are performed using ECIS-06.[12] Many local and global optical model parameters are well established for neutron and proton induced reactions. However, deuteron induced reactions require special attention due to the deuteron's weak binding energy. TALYS-2.0 provides five optical model parameters options for such cases, and in this study, the global parameters proposed by Haixia An *et al.*[13] were adopted. The optical model potential can be written as Eq. (2):

$$V(r) = -Vf_r(r) - iW_v f_v(r) + i4a_s W_s \frac{df_s(r)}{dr} + \lambda_\pi^2 (V_{so} + W_{so}) \frac{1}{r} \frac{df_{so}(r)}{dr} \vec{\sigma}.\vec{l} + V_C(r). \quad (2)$$

Here,

$$f_i(r) = \left\{ 1 + \exp\left(\frac{r - r_i A^{\frac{1}{3}}}{a_i} \right) \right\}^{-1} \quad (3)$$

with $i = r,v,s,so$ for real, volume imaginary, surface imaginary, and spin-orbit potentials respectively. Also,

$$V = V_0 + V_1 E_d + V_2 E_d^2 + V_3 \frac{N-Z}{A} + V_4 \frac{Z}{A^{1/3}}, \quad (4)$$

$$W_s = W_{s0} + W_{s1} E_d + W_{s2} \frac{N-Z}{A} + W_{s3} A^{1/3}, \quad (5)$$

$$W_v = \begin{cases} W_{v0} + W_{v1} E_d + W_{v2} E_d^2 : & E_d \le E_{bd} \\ W_{v0h} + W_{v1h} E_d + W_{v2h} E_d^2 : & E_d > E_{bd} \end{cases}, \quad (6)$$

$$R_i = r_i A^{\frac{1}{3}} \text{ with } i = r,v,s,so, \quad (7)$$

$$r_i = r_{i0} + r_{i1} A^{-1/3} \text{ with } i = r,v,s,so, \quad (8)$$

$$a_i = a_{i0} + a_{i1} A^{1/3} \text{ with } i = r,v,s,so. \quad (9)$$

Here, E_d denotes the incident deuteron energy, while *Z, N* and *A* represent the number of protons, neutrons, and nucleons of the target nucleus,[168]Er, respectively. In Eq. (4)-(6), *V* is the real part of the potential, and *Ws* and *Wv* correspond to the surface and volume absorption terms of the imaginary potential. E_{bd} defines the energy boundary in, W_V and V_c (r) is the Coulomb potential. The optimized global deuteron optical potential, developed by Haixia An *et al.*[13], is defined by 24 parameters, as listed below.

$$V = 91.85 - 0.249E_d + 0.000116E_d^2 + 0.642 \frac{Z}{A^{\frac{1}{3}}},$$

$$W_s = 10.83 - 0.0306\ E_d \text{ and } W_v = 1.104 + 0.0622\ E_d,$$

$$V_{so} = 3.557,$$

$$a_r = 0.719 + 0.0126\ A^{1/3} \text{ and } a_s = 0.531 + 0.062\ A^{1/3},$$

$$a_v = 0.855 - 0.100\ A^{1/3},$$

$$r_r = 1.152 - 0.00776\ A^{-1/3} \text{ and } r_s = 1.334 + 0.152\ A^{-1/3},$$

$$r_v = 1.305 + 0.0997\ A^{-1/3},$$

$$a_{so} = 1.011,\ r_{so} = 0.972 \text{ and } r_c = 1.303.$$

For the simulations, a continuous analysis was carried out using TALYS-2.0 to evaluate the excitation function of the [168]Er(*d,p*)[169]Er reaction. The target geometry was defined as 0.0025 mm^t × 25 mm ×25 mm. A deuteron beam current of 5 mA was assumed, with an irradiation period of 24 hours followed by a 24-hour cooling time. For nuclear mass calculations, the Gogny-Hartree-Fock-Bogoliubov model[14] was applied to assess its predictive reliability, particularly for reactions such as [169]Er production where experimental data remain unavailable.

4. Results and Discussion

The [168]Er(*d,p*)[169]Er reaction was analyzed using TALYS-2.0, and the excitation function was evaluated over a deuteron energy range of 1–200 MeV (Fig. 2). The cross-section showed a sharp rise with a maximum value of 128 mb at ~9 MeV. The effective excitation function was observed between 5 and 20 MeV. The excitation function in the 5-20 MeV range is particularly important, as it falls within the operational energies of many medium-energy cyclotrons and avoids unwanted byproducts. This energy window not only maximizes [169]Er yield but also minimizes unwanted radionuclide impurities, ensuring high activity and improved radionuclide purity. These features are critical for clinical applications in RSV, where localized delivery and minimal off-target radiation are essential. The consistency of our theoretical predictions further supports the use of this accelerator-based route as a practical and reliable method for on-site [169]Er production to meet growing clinical demand. Furthermore, results from six level density models (as mentioned in sub-section 2.2) showed minimal variation, confirming strong model consistency. For reference, the corresponding value from the TENDL-2023 nuclear data library was 123 mb[12], demonstrating good agreement between our theoretical predictions and evaluated nuclear data.

The activity-time behavior is shown in Fig. 3. During the 24-hour irradiation, activity increased steadily, reaching ~540 GBq at the end of bombardment (EOB). Following a 24-hour cooling period, activity declined exponentially with identical slopes across models, confirming a common decay constant for [169]Er. At the end of cooling, the residual activity was ~502 GBq, highlighting the production feasibility of this radionuclide.

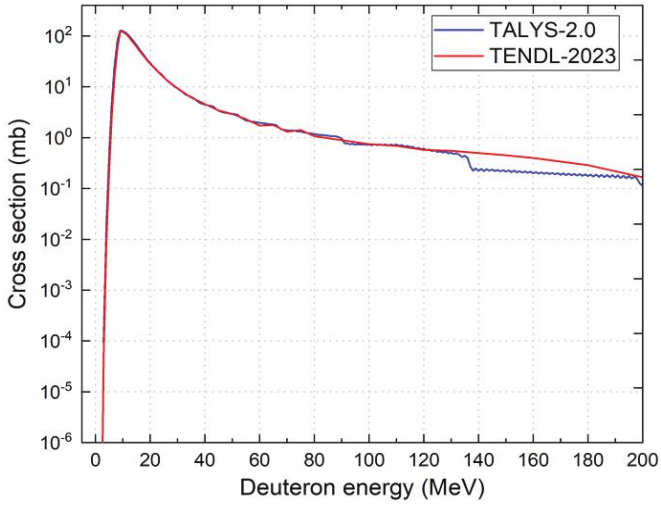

Fig. 2. Excitation function of ^{168}Er(*d,p*)^{169}Er reaction calculated with TALYS 2.0, compared with evaluated nuclear data from the TENDL-2023.[12]

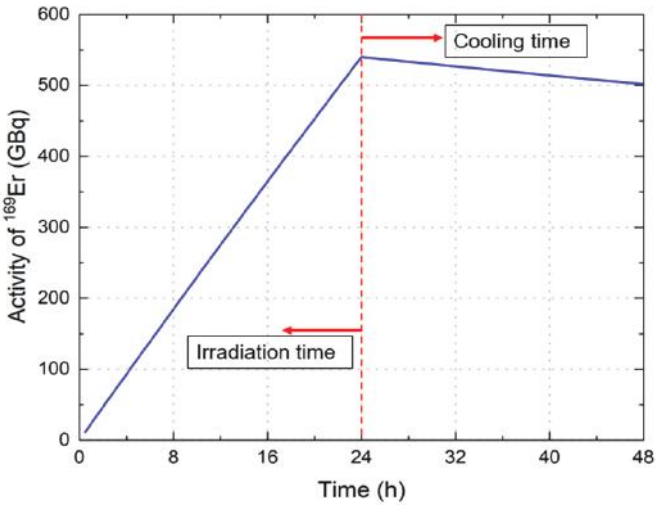

Fig. 3. Time-dependent activity of ^{169}Er radionuclide plotted with time (= irradiation time + cooling time). The red dashed vertical line separates the irradiation and cooling time during ^{169}Er production.

Moreover, the activity of ^{169}Er was evaluated as a function of incident deuteron energy for irradiation times ranging from 0 to 24 h in different time intervals. As shown in Fig. 4, the activity is primarily concentrated within the 5-20 MeV energy range, followed by a rapid decrease at higher energies. The activity peak increases proportionally with irradiation time, reaching its maximum at the end of the 24 h bombardment period. The highest activity, approximately 100 MBq, was observed at ~9 MeV, consistent with the maximum cross-section for the ^{168}Er(*d,p*)^{169}Er reaction at the same energy. Beyond ~40 MeV, the contribution to activity becomes low, indicating that the effective production window is limited to relatively low deuteron energies.

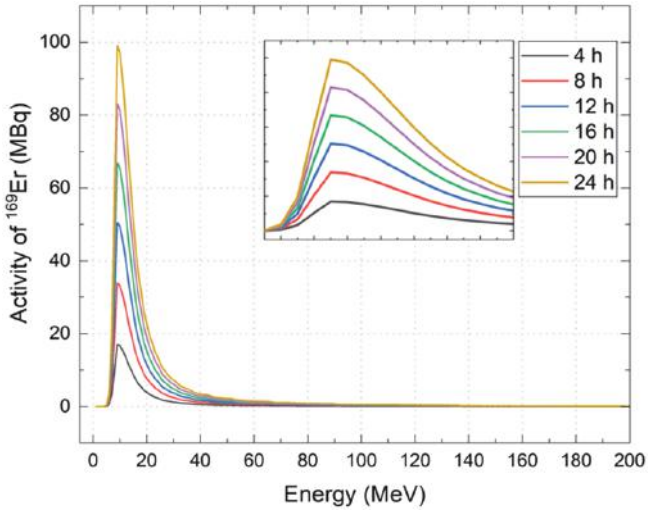

Fig. 4. Activity of ^{169}Er as a function of incident deuteron energy with different target irradiation time.

The physical yield of ^{169}Er as a function of time production is presented in Fig. 5. At EOB, the yield reached approximately 4.5 GBq/mA-h, reflecting efficient accumulation of the radionuclide. A gradual decrease was observed during the subsequent cooling period. For clinical applications, particularly in RSV, the required activity and injection volume vary with joint size.[15] Typical administered doses are 10-20 MBq for proximal or distal interphalangeal joints, 20-40 MBq for metacarpophalangeal or metatarsophalangeal joints, and 20-80 MBq for trapeziometacarpal joints.[16] These results suggest that the production levels achieved in this study are well aligned with the activity requirements for clinical use, underscoring the relevance of the proposed production scheme.

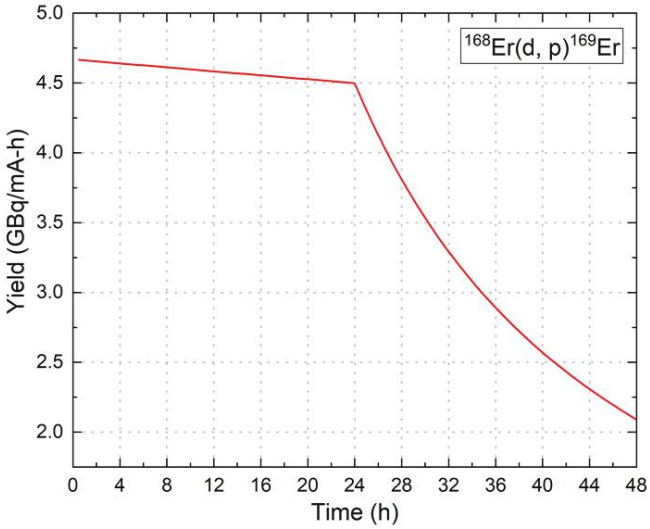

Fig. 5. Time-dependent production yield of ^{169}Er.

To evaluate the sensitivity of the results to nuclear model choices, the production yield of ^{169}Er were compared

across six level density models provided in TALYS-2.0. The results are shown in Fig. 6. The resulting production amounts at EOB are given in Table 1. Among these, the BFM model predicted the highest production and was therefore used as a reference. The GSM model showed the smallest deviation from BFM (4.68%), while SHFB exhibited the largest (15%). CTM, SHFB(C), and GHFB gave deviations of 12.92%, 14.46%, and 13.15%, respectively. Despite these differences, all models followed the same overall trend: a sharp linear increase in production up to EOB, followed by exponential decline. The moderate yet consistent variations across models indicate strong robustness of the theoretical predictions.

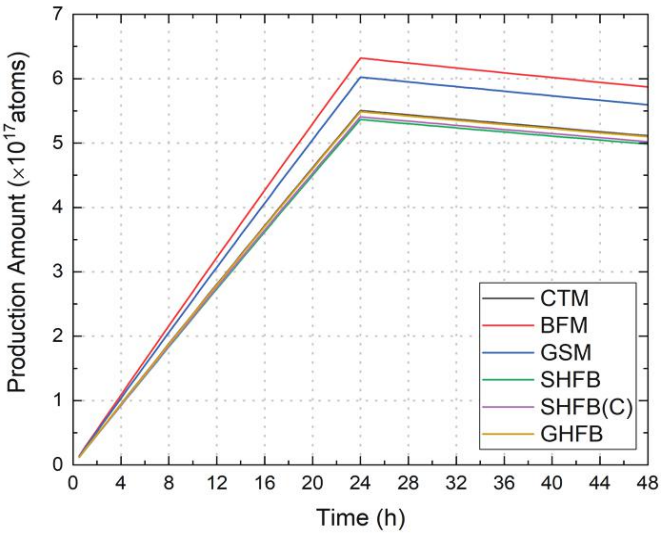

Fig. 6. Production amount versus time data of ^{169}Er for different level density models.

Table 1. Production amount of ^{169}Er at EOB.

Level density model	^{169}Er production amount (× 10^{17} atoms)
CTM	5.50
BFM	6.32
GSM	6.02
SHFB	5.37
SHFB(C)	5.41
GHFB	5.49

5. Conclusions

This study establishes that the ^{168}Er*(d,p)*^{169}Er reaction is a practical and efficient accelerator-based route for producing clinically useful ^{169}Er radionuclide. The excitation function analysis identified an optimal energy window of 5-20 MeV, with a maximum cross section of 128 mb at ~9 MeV. Under a 24-hour irradiation, the activity reached ~540 GBq at EOB, corresponding to an initial yield of ~4.6 GBq/mA-h. After a 24-hour cooling period, the activity remained ~502 GBq, confirming stability over clinically relevant timescales. Comparative analysis across six level density models showed production amounts between 5.37 × 10^{17} and 6.32 × 10^{17} atoms, with deviations less than 15% variation highlighting the robustness of the theoretical predictions. The calculated yields are more than sufficient to meet clinical requirements for RSV, where typical injection doses range from 10-80 MBq. Additionally, the favorable decay characteristics of ^{169}Er, with low-energy β^- emissions and negligible γ-ray output, ensure both therapeutic efficacy and post-RSV imaging. Overall, these findings establish a high-yield, reactor-independent, and locally deployable production pathway for ^{169}Er. Such an approach can enhance accessibility for RSV and potentially extend to palliative treatment of bone metastases, thereby supporting the broader clinical application of this important therapeutic radionuclide.

In future work, we aim to experimentally validate the calculated excitation functions and further optimize the target design to maximize production yields. These efforts will not only enhance the reliability of evaluated nuclear data libraries but also support the establishment of accelerator-based, on-site production of ^{169}Er. Such developments are expected to significantly improve the clinical availability of this radionuclide for RSV applications.

References

1. Farahati J, Elliott J, Höppner S, et al.; Post-radiosynovectomy imaging of Er-169 using scintigraphy and autoradiography, Clinical Case Reports, 5(6):1048–1050 (2017).
2. Bouchet LG, Bolch WE, Goddu SM, et al.; Considerations in the selection of radiopharmaceuticals for palliation of bone pain from metastatic osseous lesions. Journal of Nuclear Medicine, 41(4): 682–7 (2000).
3. Farahati J, Kazek S, Maric I et al.; Post-radiosynovectomy imaging utilizing Erbium-169 citrate, Applied Radiation and Isotopes, 154:108853 (2019).
4. NuDat 3, National Nuclear Data Center, Brookhaven National Laboratory, https://www.nndc.bnl.gov/nudat3/ (Retrieved on August 28, 2025).
5. Chakravarty R, Chakraborty S, Chirayil V et al.; Reactor production and electrochemical purification of 169Er: A potential step forward for its utilization in in vivo therapeutic applications, Nuclear Medicine and Biology, 41(2): 163–170 (2014).
6. Formento-Cavaier R, Köster U, Crepieux B et al.; Very high specific activity erbium 169Er production for potential receptor-targeted radiotherapy, Nuclear Instruments and Methods in Physics Research, Section B: Beam Interactions with Materials and Atoms, 463: 468–471 (2020).

7. Mughabghab SF; Thermal Cross Sections. Atlas of Neutron Resonances (6th edition), 2: 1-19 (2018).

8. Knapp FFR, Dash A; Radiopharmaceuticals for Therapy. Springer (India) Pvt. Ltd (2016).

9. Otuka N, Dupont E, Semkova V et al.; Towards a more complete and accurate experimental nuclear reaction data library (EXFOR): International collaboration between nuclear reaction data centres (NRDC), Nuclear Data Sheets, 120: 272–276 (2014).

10. Koning A, Hilaire S, Goriely S; TALYS: modeling of nuclear reactions, European Physical Journal A, 59: 131 (2023).

11. Nasrabadi, MN, Sepiani M; Study of components and statistical reaction mechanism in simulation of nuclear process for optimized production of ^{64}Cu and ^{67}Ga medical radioisotopes using TALYS, EMPIRE and LISE++ nuclear reaction and evaporation codes, AIP Conference Proceedings, 1653: 020076 (2015).

12. Koning AJ, Rochman D, Sublet JC et al.; TENDL: Complete nuclear data library for innovative nuclear science and technology, Nuclear Data Sheets, 155: 1–55 (2019).

13. An H, Cai C; Global deuteron optical model potential for the energy range up to 183 MeV, Physical Review C, 73: 054605 (2006).

14. Goriely S, Hilaire S, Girod M, et al.; The Gogny-Hartree-Fock-Bogoliubov nuclear-mass model. European Physical Journal A, 52: 202 (2016).

15. Clunie G, Fischer M; EANM procedure guidelines for radiosynovectomy, European journal of nuclear medicine and molecular imaging, 30(3): BP12–BP16 (2003).

16. Production, Quality Control and Clinical Applications of Radiosynovectomy Agents, IAEA Radioisotopes and Radiopharmaceuticals Reports No. 3, IAEA, Vienna (Austria) (2021).